iScience

CellPress
OPEN ACCESS

Article

Hypoxia inhibits the cardiac I_{K1} current through SUMO targeting Kir2.1 activation by PIP_2

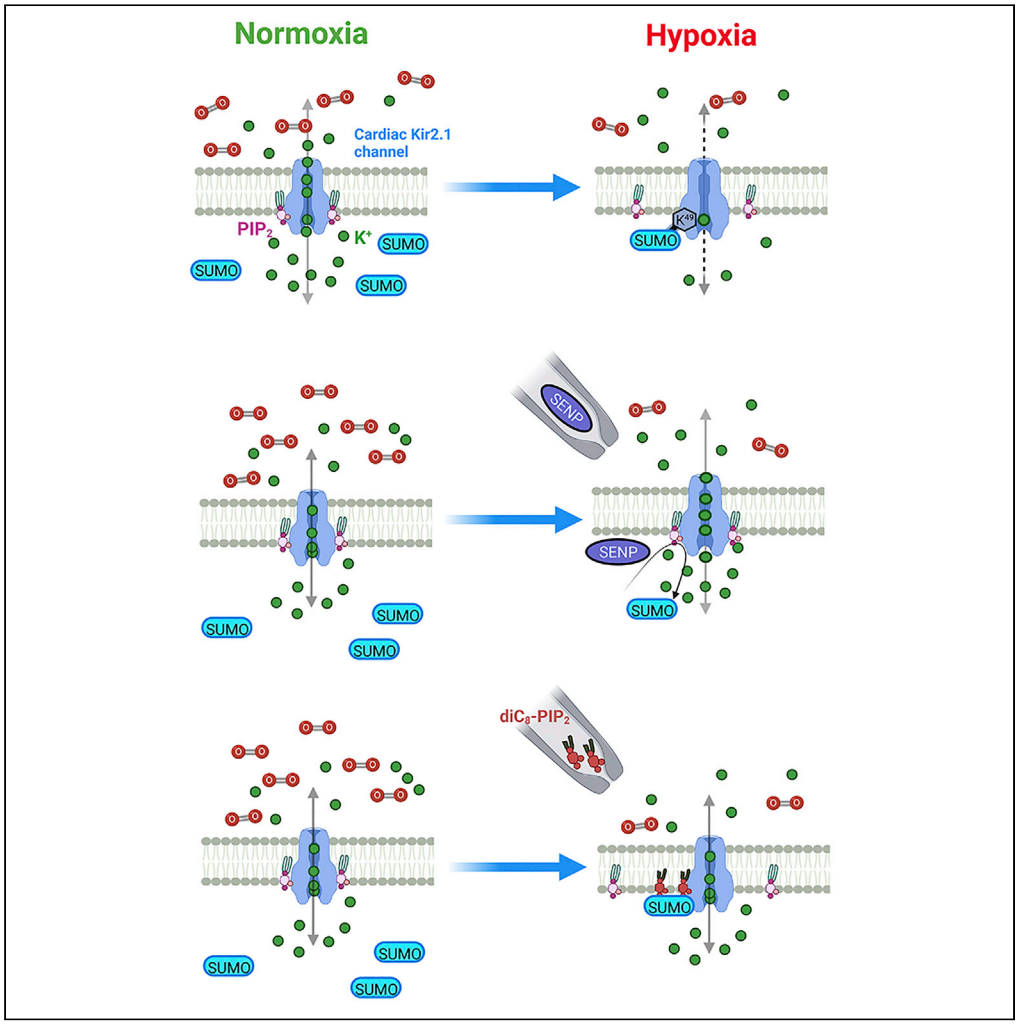

Yu Xu, Yuchen Yang, Aishwarya Chandrashekar, ..., Jenna G. Connolly, Takeharu Kawano, Leigh D. Plant

l.plant@northeastern.edu

Highlights

Acute hypoxia inhibits the inward rectifying K^+ current, I_{K1} in cardiomyocytes

Hypoxic inhibition of I_{K1} results from rapid SUMOylation of Kir2.1 channels

SUMOylation decreases the potency and efficacy of PIP_2 to activate Kir2.1 channels

An exogenous PIP_2 analog opposes hypoxic inhibition of I_{K1} and Kir2.1 channels

Xu et al., iScience 25, 104969
September 16, 2022
https://doi.org/10.1016/j.isci.2022.104969

iScience

CellPress
OPEN ACCESS

Article

Hypoxia inhibits the cardiac I_{K1} current through SUMO targeting Kir2.1 activation by PIP_2

Yu Xu,[1] Yuchen Yang,[1] Aishwarya Chandrashekar,[1] Kirin D. Gada,[1] Meghan Masotti,[1] Austin M. Baggetta,[1] Jenna G. Connolly,[1] Takeharu Kawano,[1] and Leigh D. Plant[1,2,3,*]

SUMMARY

Cardiovascular diseases remain the leading cause of death worldwide. Most deaths are sudden and occur secondary to the occlusion of coronary arteries resulting in a rapid decrease in cellular oxygen levels. Acute hypoxia is proarrhythmic, leading to disordered electrical signals, conduction block, and uncoordinated beating of the myocardium. Although acute hypoxia is recognized to perturb the electrophysiology of heart muscle, the mechanistic basis for the effect has remained elusive, hampering the development of targeted therapeutic interventions. Here, we show that acute hypoxia activates the redox-sensitive SUMO pathway in cardiomyocytes, causing rapid inhibition of the inward-rectifying K^+ channel, Kir2.1. We find that SUMOylation decreases the activation of Kir2.1 channels by the membrane phospholipid phosphatidylinositol 4,5-bisphosphate (PIP_2). These data provide a mechanistic basis for the proarrhythmic effects of acute hypoxia and offer a framework for understanding the central role of PIP_2 in mediating the sequelae of hypoxia and SUMOylation in cardiovascular disease.

INTRODUCTION

The heart has the highest basal oxygen (O_2) consumption per unit mass of any organ in the body and is exquisitely dependent on aerobic metabolism to maintain regular contractility and pumping throughout life. Disrupting the myocardial O_2 supply initiates a pathophysiological chain reaction that can include the rapid onset of arrhythmia and conduction block (Sattler et al., 2019). Although acute myocardial hypoxia has been the subject of intense investigation since the early 1900s, the mechanistic basis for hypoxia-induced arrhythmia is unresolved (Austen et al., 1963).

We recently reported that SUMOylation is upregulated in response to acute hypoxia, mediating a rapid increase in the excitability of neurons and iPS-derived cardiomyocytes (Plant et al., 2016, 2020). SUMOylation is a ubiquitous post-translational modification pathway that controls the activity of multiple transcription factors and a growing cadre of extranuclear target proteins (Henley et al., 2018). SUMOs are ubiquitin-like proteins that require a stepwise enzymatic pathway to operate. Following ATP-dependent activation, SUMOs attach to the E2-ligase Ubc9 via a thiol-linkage, rendering the pathway responsive to the redox status of the cell (Xu et al., 2008). Ubc9 then mediates the conjugation of SUMO-subunits to the ε-amino group of specific lysine residues localized to the second position of the canonical SUMOylation motif, Ψ-K-X-E/D, on a target protein. SUMOylation is readily reversed by the action of SENP deSUMOylases that cleave the isopeptide bond between SUMO and the target protein. Thus, despite covalent linkage to target proteins, SUMOylation is highly dynamic and labile (Hay, 2005). This facet of SUMOylation is commonly observed with ion channels, where the activity of the SUMO-pathway has been shown to increase cellular excitability via the suppression of K_{2P} or K_V channels, or by augmenting the activity of Na_V channels (Plant et al., 2011, 2020; Xiong et al., 2017).

The inward rectifying K^+ current I_{K1} stabilizes the resting membrane potential of ventricular cardiomyocytes and shapes both the initial depolarization and final repolarization of the cardiac action potential (Dhamoon and Jalife, 2005). I_{K1} is passed predominantly by the classical inward rectifying K^+ channel Kir2.1, with contributions from Kir2.2 and Kir2.3 (Zaritsky et al., 2001). Mutations or perturbation to the function of I_{K1} are associated with multiple arrhythmic phenotypes, including Andersen-Tawil syndrome (also called Long QT syndrome type 7), Short QT syndrome type 3, atrial fibrillation, catecholaminergic polymorphic ventricular tachycardia, supraventricular tachycardia, and ventricular fibrillation (Tawil et al., 1994). Indeed, modulation

[1]Department of Pharmaceutical Sciences, School of Pharmacy and Pharmaceutical Sciences, Bouvé College of Health Sciences, Northeastern University, Boston, MA, USA

[2]Center for Drug Discovery, Northeastern University, Boston, MA, USA

[3]Lead contact

*Correspondence: l.plant@northeastern.edu

https://doi.org/10.1016/j.isci.2022.104969

of I_{K1} has been proposed as a preventative strategy in patients predisposed to specific arrhythmic phenotypes (Dhamoon and Jalife, 2005). All Kir channels, including Kir2s, require the membrane phospholipid phosphatidylinositol 4,5-bisphosphate (PIP_2) to maintain activity. Although PIP_2 is a minor component of the plasma membrane, it is so central as a required cofactor for Kir2 function, that many disease mutations and channel regulators act by altering the interaction between PIP_2 and the channel protein (Liang et al., 2014; Logothetis et al., 2015; Lopes et al., 2002).

Despite the recognized need to identify tractable molecular mechanisms that could be leveraged to suppress the proarrhythmic effects of acute myocardial hypoxia, the role of hypoxia and SUMOylation in regulating I_{K1}, or Kir2 channels remains unknown. Here, we combine electrophysiology with optogenetic and spectroscopic probes to show that acute hypoxia initiates rapid SUMOylation of Kir2.1 channels in cardiomyocytes. We find that SUMO1 inhibits I_{K1} by reducing the potency of PIP_2-mediated activation of Kir2.1 channels.

RESULTS

Hypoxia inhibits I_{K1} in cardiomyocytes

The effects of acute hypoxia on I_{K1} in rat ventricular cardiomyocytes (RVCMs) were studied by voltage-clamp recording in the whole-cell mode. Reducing the O_2-tension of the superfusate from ambient levels to 2% O_2 resulted in a rapid 40 $\pm$ 0.1% (mean $\pm$ SD) decrease in I_{K1} of over 90 s. Both the hypoxia-sensitive and insensitive components of the current were blocked by Ba^{2+} (3 mM), consistent with the known role of Kir2 channels in mediating I_{K1} (Figure 1A) (Liang et al., 2014).

We previously demonstrated that acute hypoxic challenge rapidly increases the SUMOylation of $Na_V1.2$ and $Na_V1.5$ channels in cerebellar neurons and iPS-derived cardiomyocytes, respectively (Plant et al., 2016, 2020). To determine if SUMOylation mediates the hypoxic inhibition of I_{K1} in RVCMs, we introduced purified SENP1 (2 μM) to the cytosol via the recording pipette. SENP1 increased I_{K1} by 17.6 $\pm$ 6.5%, indicating that the current was partially inhibited by SUMOylation under resting conditions, as observed with other membrane localized SUMO-target proteins (Plant et al., 2016; Xiong et al., 2017). Furthermore, treatment with SENP1 rendered I_{K1} insensitive to hypoxia (Figures 1A and 1B). In contrast, when we included SUMO1 (1 μM) in the recording pipette, a maneuver that increases SUMO-conjugation to ion channels, I_{K1} decreased by 48 $\pm$ 8% and the hypoxia-sensitive component of the current was abolished (Figure 1B). Both the SUMO1 and hypoxia-mediated inhibition of I_{K1} remained stable throughout the remainder of the experiment (up to ten minutes, not shown). Together, these results suggest that SUMOylation mediates the hypoxia-induced inhibition of I_{K1} in RVCMs.

Next, we sought to determine if, in addition to precluding the effects of hypoxia, SENP1 could reverse hypoxic inhibition of I_{K1}. To accomplish this, we developed an optogenetic tool that allows spatiotemporal control of SENP1 recruitment to the plasma-membrane based on a robust platform that allows control of the membrane localization of proteins of interest (Gada et al., 2022; Idevall-Hagren et al., 2012; Ningoo et al., 2021; Xu et al., 2020). Briefly, we fused SENP1 to the photolyase homology domain of cryptochrome 2 (CRY2) and co-expressed this construct with the transcription factor cryptochrome-interacting basic-helix-loop-helix N-terminal fragment (CIBN), which localizes to the plasma membrane via a CAAX motif. Upon stimulation with 460 nm light, CRY2 binds to CIBN resulting in nearly instantaneous recruitment of SENP1 to the plasma membrane. This maneuver reversed the hypoxia-induced inhibition of I_{K1} within ~180 s despite prolonged exposure of RVCMs to hypoxia. Indeed, the activation of CRY2-SENP1 increased I_{K1} by 11 $\pm$ 4% above pre-hypoxic values, consistent with partial SUMO-inhibition of the current under ambient conditions (Figure 1C). CRY2-SENP1 did not alter the magnitude of I_{K1} in RVCMs studied with purified SENP1 in the recording pipette (Figure 1C).

SUMO1 inhibits Kir2.1 but not Kir2.2 or Kir2.3

Sequence analysis of the three Kir2 channels that mediate I_{K1} identified a single putative SUMO-site in Kir2.1 (V-K_{49}-K-D) located in the N-terminal domain of the channel, proximal to the interface with the plasma membrane. An analogous site is present in Kir2.2 and Kir2.3 but has an asparagine at the fourth position (V-K-K-N; Figure 2A), rather than an acidic residue that would mediate efficient SUMOylation. To study the association between Kir2 channels and SUMO1, we heterologously expressed them and measured donor-decay Förster Resonance Energy Transfer (FRET), as before (Plant et al., 2011, 2016), between subunits tagged with the fluorescent proteins mTFP1-Kir2 and YFP-SUMO at the surface of HEK293T cells. mTFP1-Kir2.1 was visualized at the cell membrane

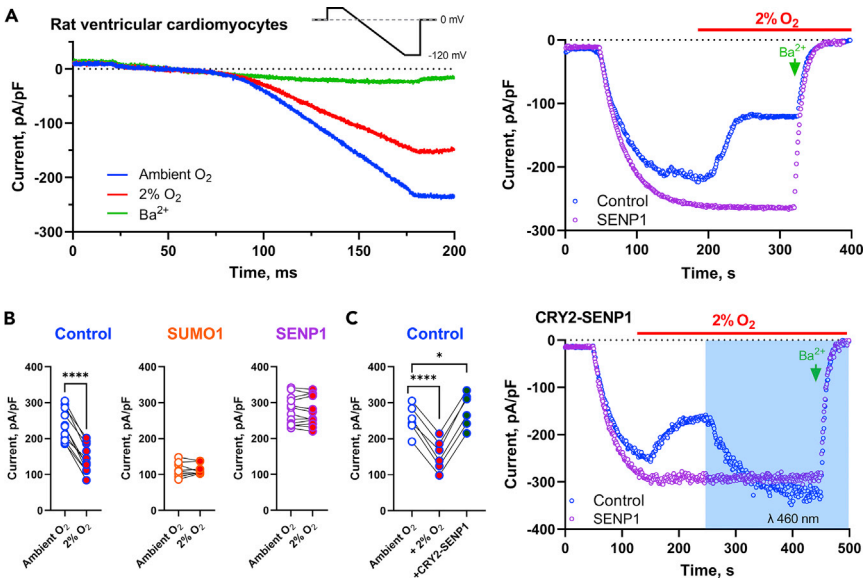

Figure 1. Acute hypoxia inhibits I_{K1} via SUMOylation

I_{K1} in rat ventricular cardiomyocytes (RVCMs) was studied by the whole-cell patch-clamp. Currents were evoked in a high external K^+ recording buffer and measured at −120 mV, as described in the STAR Methods. Hypoxia was a drop in O_2 from ambient levels to 2% (red), measured at the cell. The time-course of hypoxic inhibition was studied by recording the magnitude of I_{K1} every second. Cells were studied with the following pipette solutions: control (blue), SUMO1 (1 μM, orange), or SENP1 (2 μM, magenta). CRY2-SENP1 was targeted to the cell membrane by the activation of a 460 nm LED during the time period indicated. I_{K1} currents were blocked by the addition of 3 mM Ba^{2+} (green).

(A) Exposure to acute hypoxia (2% O_2) inhibits ~40% of I_{K1} in RVCMs. *Left*, representative current sweeps; *right*, a representative time course showing the kinetics of hypoxic inhibition in RVCMs studied with a control pipette solution. The inhibition is precluded by including SENP1 (2 μM) in the recording pipette. The reverse ramp recording protocol is inset.

(B) Including SUMO1 (1 μM) in the recording pipette inhibits I_{K1} and precludes the effects of hypoxia. SENP1 augments I_{K1} and protects the current from hypoxia. Data are from 8 to 10 RVCMs per group, ****p < *0.0001*, paired, two-tailed Student's *t* test.

(C) Hypoxic inhibition of I_{K1} was reversed by the activation of CRY2-SENP1 with 460 nm light (cyan box) when RVCMs are studied with a control pipette solution. *Right*, CRY2-SENP1 does not alter current when 2 μM SENP1 is included in the recording pipette. Data are from 6 RVCMs, *p < *0.05*, ****p < *0.0001*, paired, two-tailed Student's *t* test.

and photobleached under continual illumination with a time constant (τ_{decay}) of 63.6 ± 9 s in the presence of untagged YFP. The τ_{decay} increased by 71.2 ± 4% when mTFP1-Kir2.1 was studied with co-expressed YFP-tagged SUMO1, consistent with a stable protein-protein interaction, i.e. SUMOylation (Figures 2B and 2C). Confirmation that SUMOylation of Kir2.1 occurs at K49 was obtained by studying channels with point mutations in the SUMO-motif. Thus, FRET was not observed in mTFP-Kir2.1-K49Q or K49R channels that lack the lysine at position 49, or with mTFP-Kir2.1-D51N channels that lack an acidic residue in the fourth position of the motif (Figure 2C). These findings indicate that both the target lysine and the terminal acidic residue in the Ψ-K-X-D motif, are critical for the SUMOylation of Kir2.1, as predicted. Thus, YFP-SUMO1 did not is-ci_104969_fx1_3c.tif - FRET with either mTFP-tagg - d Kir2.2 or Kir2.3, which both lack the terminal acidic residue of the motif. However, FRET between mTFP1-tagged Kir2.2 or Kir2.3 and SUMO1 was enabled by replacing the asparagine at position four of either channel with aspartic acid to generate mTFP1-Kir2.2-N50D and mTFP1-Kir2.3-N25D, respectively (Figures 2D and 2E).

The valine in the first position of the SUMO-motif (Kir2.1-V48) is conserved in Kir2 channels and is present in 11 out of 16 Kir channels. The lysine in the third position of the motif (Kir2.1-K50) is absolutely conserved among Kir channels and is recognized to coordinate with PIP_2 (Cui et al., 2021). We studied the role of V48 and K50 in the SUMOylation motif using two-electrode voltage clamp (TEVC) to measure channel currents and FRET to assess SUMO interactions. First, we tested Kir2.1-K48L, a mutation that preserves the hydrophobic character of the ψ residue in the first position of the motif. Of note, leucine is found in this po-sition in Kir4.1 and Kir5.1 channels (Cui et al., 2021). In accord with SUMO-regulation, Kir2.1-V48L currents

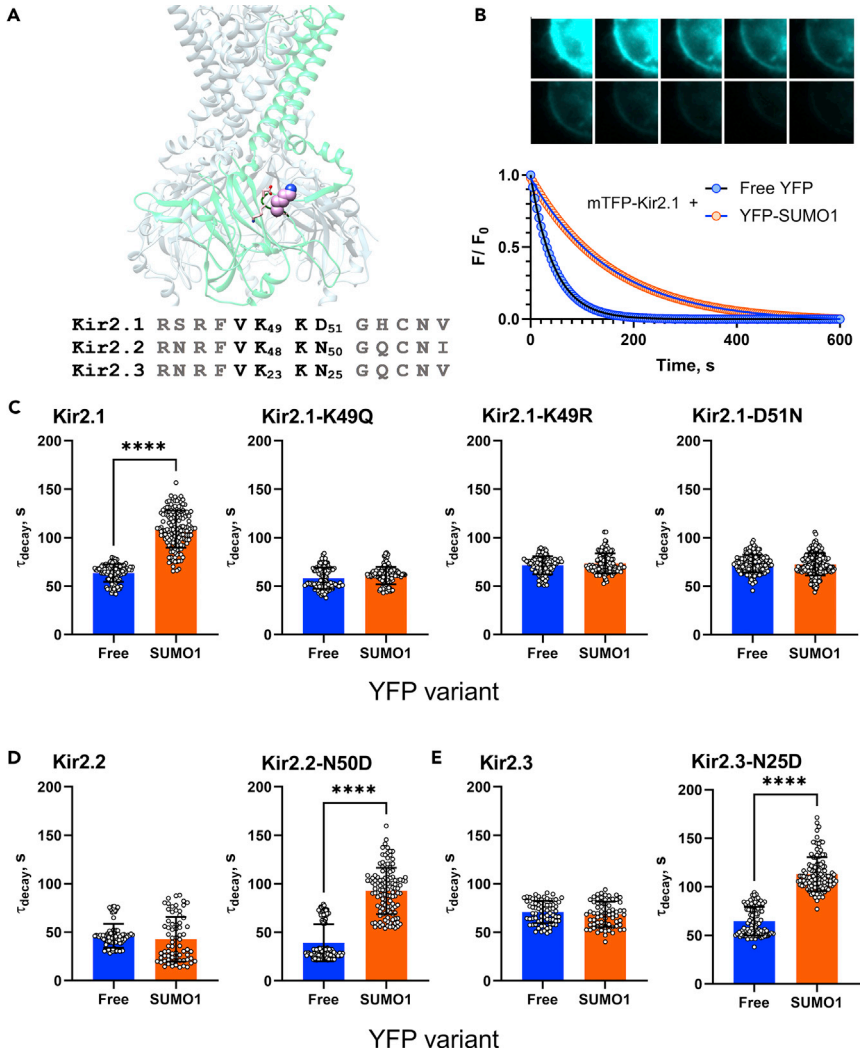

Figure 2. SUMOylation regulates Kir2.1 at lysine 49

Rat Kir2.X channels were studied in live HEK293T cells, per the STAR Methods. Donor-decay photobleaching FRET was assessed by measuring the time constant (τ_{decay}) for mTFP photobleaching (donor) in the presence of YFP (acceptor). Data are mean ± s.d. for n = 70-150 bleaching curves per condition, ****p < *0.0001*, unpaired, two-tailed Student's *t* test. See also Figure S1.

(A) *Upper*, a schematic of the SUMOylation motif in Kir2.1 created using UCSF Chimera (Pettersen et al., 2004). The channel is a tetramer and one subunit is shown in green. The SUMOylation motif is shown as ball and stick, with lysine-49 shown as a space-filled residue. *Lower*, the NCBI sequences of rat Kir2.1, Kir2.2, and Kir2.3 are shown with the SUMO-target lysine in the second position of the motif numbered. Note that Kir2.2 and Kir2.3 lack the critical aspartic acid in the fourth position of the canonical motif Ψ-K-X-E/D.

(B) *Upper*, montage of mTFP-Kir2.1 photobleaching in an example HEK293T cell. *Lower*, example donor-decay photobleaching curves in the presence and absence of YFP (free) or YFP-SUMO1.

(C) YFP-SUMO1 FRETs with mTFP-tagged Kir2.1 but not Kir2.1-K49Q, K49R, or D51N channels.

(D) YFP-SUMO1 does not FRET with Kir2.2 but does FRET with Kir2.2-N50D channels.

(E) YFP-SUMO1 does not FRET with Kir2.3 but does FRET with Kir2.3-N25D channels.

were reduced by ~38% in *Xenopus laevis* oocytes co-expressing SUMO1 and Ubc9. Similarly, FRET was observed between YFP-tagged SUMO1 and mTFP1-Kir2.1-V48L channels in HEK293T cells, consistent with SUMOylation (Figures S1A and S1B). In contrast, both FRET with SUMO1, and the functional effects of SUMOylation were absent when V48 was substituted for a hydrophilic residue (Kir2.1-V48Q; Figure S1C). K50 is conserved among Kir channels and in Kir2.1 is located in the third, "X" position of the SUMO-motif. Therefore, SUMOylation of Kir2.1 is expected to occur irrespective of mutations that would alter the

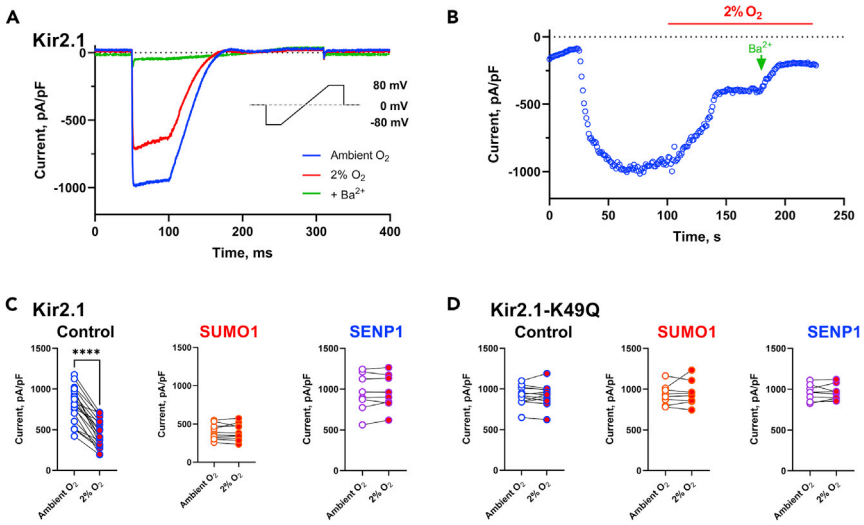

Figure 3. Lysine 49 is required for hypoxic inhibition of Kir2.1

Rat Kir2.1 channels were expressed in HEK293T cells and studied by whole-cell patch-clamp recording with the following pipette solutions: control (blue) SUMO1 (1 μM, orange) or SENP1 (2 μM, magenta). Currents were evoked using a high K^+ recording buffer and were measured at −80 mV, as described in the STAR Methods using a ramp protocol (inset). Hypoxia (red) was a drop in O_2 from ambient levels to 2%, measured at the cell. Kir2.1 channel currents are blocked by the addition of 3 mM Ba^{2+} (green). The time course of hypoxic- inhibition was studied by recording the magnitude of I_{K1} every second. See also Figure S2.

(A) Representative sweeps showing hypoxic inhibition of Kir2.1 channels.

(B) A representative time course showing that Kir2.1 is inhibited by hypoxia.

(C) Including SUMO1 in the recording pipette decreases Kir2.1 currents and prevents further inhibition by hypoxia, while SENP1 augments the current and precludes the effects of hypoxia. Data are from 8 to 12 cells per group, ****$p < 0.0001$, paired, two-tailed Student's *t* test.

(D) Kir2.1-K49Q channels are insensitive to regulation by hypoxia or inclusion of SUMO1 or SENP1 in the recording pipette. Data are from 8 to 12 cells per group.

biochemical character of the residue at this position. Consistent with this prediction, FRET and TEVC experiments showed that Kir2.1-K50A, K50Q, and K50R channels are all subject to SUMO-regulation (Figures S1D–S1F).

Next, we used whole-cell patch-clamp recording to study the functional effects of hypoxia and SUMOylation on Kir2 channels heterologously expressed in HEK293T cells. Acute hypoxia inhibited Kir2.1 currents by 44.1 ± 4%. Like I_{K1}, including SENP1 in the recording pipette augmented Kir2.1 currents by 20 ± 3% and abolished the inhibitory effect of hypoxia while SUMO1 decreased the currents by 51.2 ± 4% and precluded hypoxic inhibition (Figures 3A-3C). In contrast, Kir2.1-K49Q channel currents did not respond to hypoxia, exogenous SENP1, or SUMO1 peptides and exhibited basal currents that were 18 ± 3% larger than those recorded from wild-type Kir2.1 channels (Figure 3D). Of note, neither Kir2.2 or 2.3 channels were regulated by acute hypoxia (Figure S2).

SUMO interferes with Kir2.1 activation by PIP_2

The gating of Kir2 channels is highly dependent on interactions with PIP_2 (Logothetis et al., 2015). We have previously shown that the mechanistic action of channel regulators that operate by allosterically altering channel-PIP_2 interactions can be studied using optogenetic activation of inositol 5-phosphatase to rapidly dephosphorylate PIP_2 in voltage-clamped cells (Ningoo et al., 2021; Xu et al., 2020). To accomplish this, *Xenopus laevis* oocytes are co-injected with the channel, CRY2-5′ptase$_{OCRL}$ (5′ptase), and the membrane anchor CIBN-CAAX. Activation of the optogenetic system by 460 nm light results in the rapid recruitment of 5′ptase to the cell membrane, leading to 5′-dephosphorylation of PIP_2 and the generation of PI(4)P, a phospholipid species that does not support efficient gating of Kir2.1 channels (Rohacs et al., 1999). Activation of 5′ptase inhibited 57.1 ± 4% of the Kir2.1 current in a mono-exponential fashion, with a time constant (tau) of 812 ± 60 s (Figures 4A-4C). Heterologous expression of SUMO1 decreased basal Kir2.1 currents by 25 ± 2% and augmented both the magnitude and the rate of current inhibition observed following the

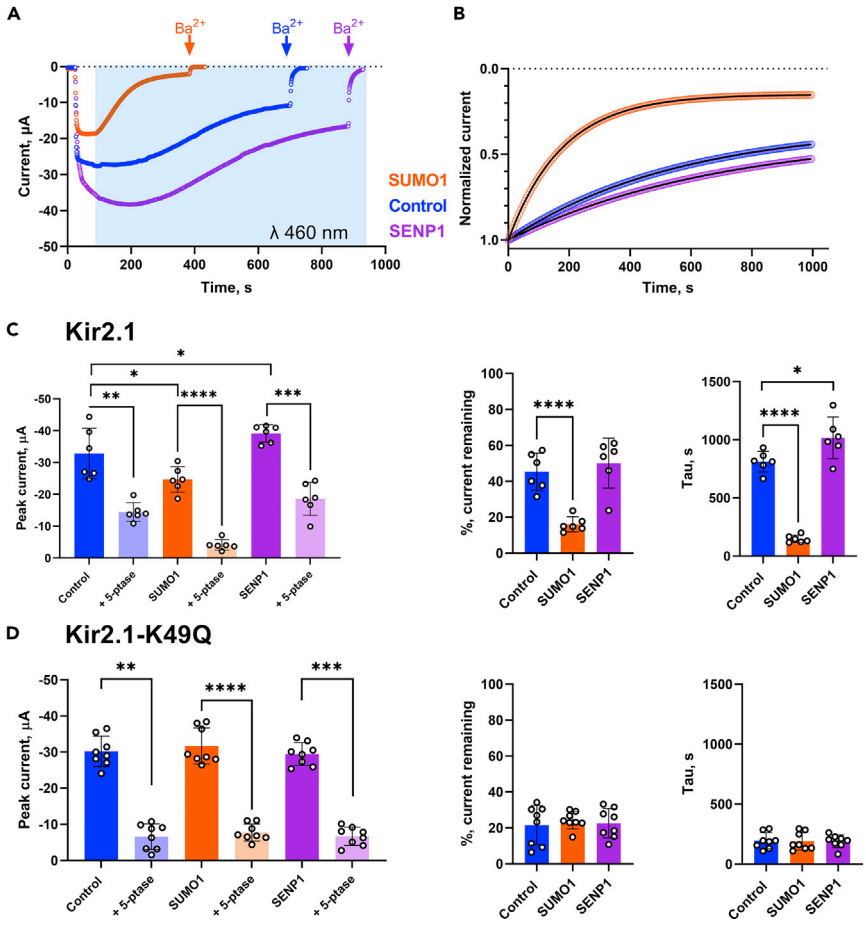

Figure 4. SUMO1 decreases the effect of PIP_2 on Kir2.1

Rat Kir2.1 channel currents were studied in *Xenopus* oocytes by two-electrode voltage-clamp. Currents were evoked in a high external K^+ recording buffer and measured at −80 mV, as described in the STAR Methods. To study the effects of SUMOylation and deSUMOylation, the oocytes were also injected with cRNAs expressing Ubc9 and SUMO1 (orange) or SENP1 (magenta) and compared to control oocytes (blue). Endogenous PIP_2 was dephosphorylated at the 5′ position by co-expressing CIBN-CAAX and CRY2-5′ptase$_{OCRL}$.(5′ptase) and activating this optogenetic system with a 460 nm LED were indicated by the cyan box. Data are mean ± s.d. for 6-8 oocytes per group, *p < *0.05*,**p < *0.01*, ***p < *0.001*, ****p < *0.0001*, paired, two-tailed Student's *t* test; *p < *0.05*, unpaired, two-tailed Student's *t* test. See also Figures S3–S6.

(A) Example time courses show that the rate of inhibition of Kir2.1 by the activation of CRY-5′ptase is increased by SUMO1 and slowed by SENP1.

(B) The tau of inhibition is determined by fitting the data with a mono-exponential function.

(C) *Left*, Summary data showing the effect of co-expressed SUMO1 or SENP1 on the peak Kir2.1 current before and after the activation of 5′ptase as well as the percentage of the current remaining (*middle*) and the tau of inhibition (*right*).

(D) *Left*, Summary data showing that co-expression of SUMO1 or SENP1 does not alter peak Kir2.1-K49Q current before and after the activation of 5′ptase. The percentage of Kir2.1-K49Q current remaining (*middle*) and the tau of inhibition (*right*) are insensitive to SUMO1 or SENP1.

activation of 5′ptase. Together, these data suggest that SUMOylation decreases the activity of Kir2.1 by interfering with channel-PIP_2 interactions. This interpretation is supported by additional studies using this experimental system. First, co-expression of SENP1 enhanced Kir2.1 currents by 20 ± 3% and reduced both the magnitude and the rate of current inhibition by 5′ptase (Figures 4A-4C). Second, Kir2.1-K49Q, K49R, or D51N channel currents were unaltered by co-expression of SUMO1 or SENP1, and neither SUMO1 nor SENP1 modulated the extent or the tau of current inhibition following the activation of 5′ptase (Figures 4D and S3). Of note, the relative activity of 5′ptase was greater in Kir2.1-K49Q than in K49R channels, an observation that we attribute to increased stabilization of PIP_2 when the residue at position 49 has a positive charge (lysine or arginine). Similarly, activation of 5′ptase resulted in efficient inhibition of Kir2.2 and 2.3 channels in a manner that was not altered by co-expression of SUMO1 or SENP1 (Figure S4).

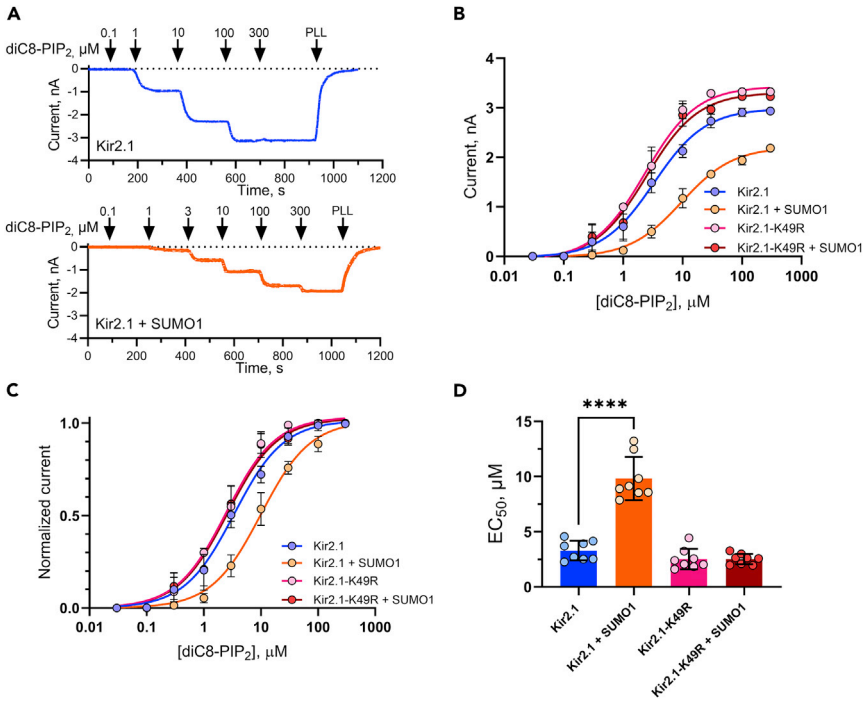

Figure 5. SUMOylation interferes with the activation of Kir2.1 channels by diC8-PIP_2

Kir2.1 or Kir2.1-K49R channels were expressed in *Xenopus* oocytes with or without Ubc9 and SUMO1 and the currents from excised macropatches were studied by patch-clamp recording at −100mV. See the STAR Methods for experimental details. Data are mean ± s.d. for 7-9 experiments per condition. ****p < *0.0001*, paired, two-tailed Student's *t* test.

(A) Example data showing that Kir2.1 (blue, *upper*) or Kir2.1-K49R (orange, *lower*) channels were first exposed to poly-L-lysine (PLL; 20 μg/mL, not shown) and then to increasing concentrations of diC8-PIP_2, as indicated. Currents were then deactivated by re-exposure to PLL. Patches were studied with multiple concentrations of diC8-PIP_2 always including 10 μM as a reference.

(B) Mean current magnitudes plotted against the concentration of diC8-PIP_2.

(C) The data are normalized to obtain EC_{50} values.

(D) Summary data show that diC8-PIP_2 activates Kir2.1 with a mean EC_{50} of 3.3 ± 1 μM. The EC_{50} increases to 9.8 ± 2 μM when patches were excised from oocytes overexpressing SUMO1 and Ubc9. DiC8-PIP_2 activated Kir2.1-K49R with an EC_{50} of 2.5 ± 1 μM with or without co-expression of SUMO1.

However, Kir2.2-N50D and Kir2.3-N25D channels were observed to be SUMO1-sensitive, exhibiting currents that were diminished by co-expression of SUMO1 and augmented by SENP1 (Figure S5). Together, these data suggest that SUMOylation decreases Kir2.1 current by interfering with interactions between the channel and PIP_2 that are required for efficient gating.

To further characterize the role of PIP_2 in mediating the effects of SUMOylation on Kir2.1 channel function, we studied inside-out macropatches excised from *Xenopus laevis* oocytes expressing Kir2.1 or Kir2.1-K49R with, or without Ubc9 and SUMO1 (Figure 5). In this experiment, the inside surface of the patch is treated first with poly-L-lysine (20 μg/mL). This procedure chelates endogenous phosphoinositides, including PIP_2 and thereby prevents Kir2.1 activity. Next, the patches are exposed to diC8-PIP_2, a water-soluble analog of PIP_2 with eight-carbon long acyl chains to study the concentration-dependence of diC8-PIP_2-mediated Kir2.1 channel activation (Figures 5A-5C). In accord with prior studies, diC8-PIP_2 activated Kir2.1 channels with a half-maximal value (EC_{50}) of 3.3 ± 1 μM (mean ± s.d.) (An et al., 2012). When Kir2.1 was co-expressed with Ubc9 and SUMO1 the EC_{50} value for diC8-PIP_2 activation was significantly right-shifted to 9.8 ± 2 μM (Figure 5D). In contrast, the mean EC_{50} for diC8-PIP_2 to reactivate Kir2.1-K49R was 2.5 ± 1 μM whether or not SUMO1 was co-expressed (Figure 5D). These data verify that SUMO1 impairs the ability of diC8-PIP_2 to activate Kir2.1 channels.

To exclude the possibility that PIP_2 is required to mediate SUMO-conjugation to Kir2.1, we assessed FRET between mTFP-tagged Kir2.1 and YFP-SUMO1 in cells treated with wortmannin, a fungal sterol that at

micromolar concentrations inhibits the PI4 kinases required to generate PIP_2. Following a 2-h treatment with wortmannin (10 μM), FRET was still observed between mTFP1-Kir2.1 and YFP-SUMO1 but not between mTFP1-Kir2.1-K49Q and YFP-SUMO1. These data show that the SUMOylation of Kir2.1 is not dependent on PIP_2 (Figure S6).

Exogenous diC8-PIP_2 blunts hypoxic inhibition of I_{K1}

To confirm that hypoxic inhibition of I_{K1} is primarily mediated by SUMOylation of Kir2.1, we transduced RVCMs with lentivirus expressing shRNAs targeted against mRNA transcripts of KCNJ2, the gene that encodes Kir2.1. Individual Kir2.1^{kd}-CMs were identified by the expression of eGFP from bicistronic lentiviral particles and studied by patch-clamp recording. In comparison to cells expressing the scrambled shRNA, I_{K1} was decreased by 72 ± 9% in Kir2.1^{kd}-CMs. Furthermore, the residual I_{K1} in Kir2.1^{kd}-CMs was insensitive to hypoxia, SUMO1, or SENP1 (Figures 6A and 6B). Together, these data show that hypoxic inhibition of I_{K1} requires Kir2.1.

Next, we showed that adding diC8-PIP_2 into the patch-pipette opposes hypoxic inhibition of I_{K1}. Including diC8-PIP_2 in the pipette diminished the hypoxic inhibition of I_{K1} in a concentration-dependent manner in wild-type RVCMs, with 100 μM diC8-PIP_2 reducing hypoxic inhibition of I_{K1} from ~40% to ~15%. The same result was observed in cells transduced with the scrambled shRNA but was abolished in Kir2.1^{kd}-CMs (Figure 6C). Adding diC8-PIP_2 in the recording pipette also produced a concentration-dependent reduction in hypoxic inhibition of heterologous Kir2.1 channels expressed in HEK293T cells. As before, the effects of hypoxia were ameliorated by SENP1 (2 μM) and were not observed in Kir2.1-K49Q channels (Figure 6D).

We visualized and quantified the interactions between native Kir2.1 and SUMO1 in RVCMs using the proximity-ligation association (PLA) assay. Proximity ligation requires establishing the specificity of the primary antibodies that will be used in the assay. To accomplish this, we tested the specificity of antibodies against Kir2.1, Kir2.2, and Kir2.3 channels heterologously expressed in HEK293T cells (Figure S7). Because our functional studies predict that only up to ~20% of Kir2.1 channels are SUMOylated at baseline we do not anticipate visualizing the small population of SUMO-adducts under these experimental conditions. The validated Kir2 antibodies were paired with SUMO1 antibodies that we have tested and utilized before (Plant et al., 2011). Under control conditions, interactions were observed between Kir2.1 and SUMO1, but not between Kir2.2 or Kir2.3 and SUMO1. Exposing RVCMs to acute hypoxia resulted in a significant increase in the number of interactions between native Kir2.1 and SUMO1 consistent with the conclusion that hypoxia-augments the SUMOylation of Kir2.1 channels in cardiomyocytes (Figures 6E and S7).

Although cardiomyocytes are typically cultured at 21% O_2, the oxygen level in the myocardium is estimated to be in the range of 5-10% O_2, under physiological conditions (Roy et al., 2003). Therefore, we studied the impact of acute hypoxia on I_{K1} in RVCMs cultured at 7% O_2. Culturing RVCMs at 7% O_2 diminished I_{K1} by ~75% to a mean density of −40 ± 14 pA/pF (n = 5). However, the current remained sensitive to acute hypoxia, showing a rapid, ~25% inhibition upon exposure to 2% O_2 (Figure S8). Next, we used PLA to study interactions between Kir2.1 and SUMO1 in RVCMs cultured at 7% O_2. Although culturing RVCMs at 7% O_2 reduced I_{K1} we did not observe a concurrent change in the frequency of Kir2.1-SUMO1 PLA interactions compared to cells cultured at 21% O_2. This finding argues that the decrease in basal I_{K1} cannot be attributed to SUMOylation. As expected, based on our electrophysiological data, exposing RVCMs cultured at 7% O_2 to 2% O_2 evoked an increase in the frequency of PLA interactions, consistent with hypoxia-induced SUMOylation of Kir2.1 (Figure S8).

DISCUSSION

Perturbation of I_{K1} is recognized to evoke multiple phenotypes of cardiac arrhythmia. This study establishes that acute hypoxia inhibits I_{K1} in cardiomyocytes by reducing the potency of PIP_2 to act as a required cofactor for the activation of Kir2.1 channels. These data offer a framework for understanding the central role of PIP_2 in opposing the proarrhythmic effects of hypoxia and SUMOylation in the myocardium.

Here, we identify Kir2.1 as a SUMO-target protein in ventricular cardiomyocytes. SUMOylation occurs within minutes of the onset of hypoxia and inhibits Kir2.1 channel function, consistent with the induction of cardiac arrhythmia in hypoxic or anoxic myocardium (Sattler et al., 2019) and prior studies in heterologous cells, neurons, and iPS-derived cardiomyocytes, (Plant et al., 2016, 2020) a cardiac model system

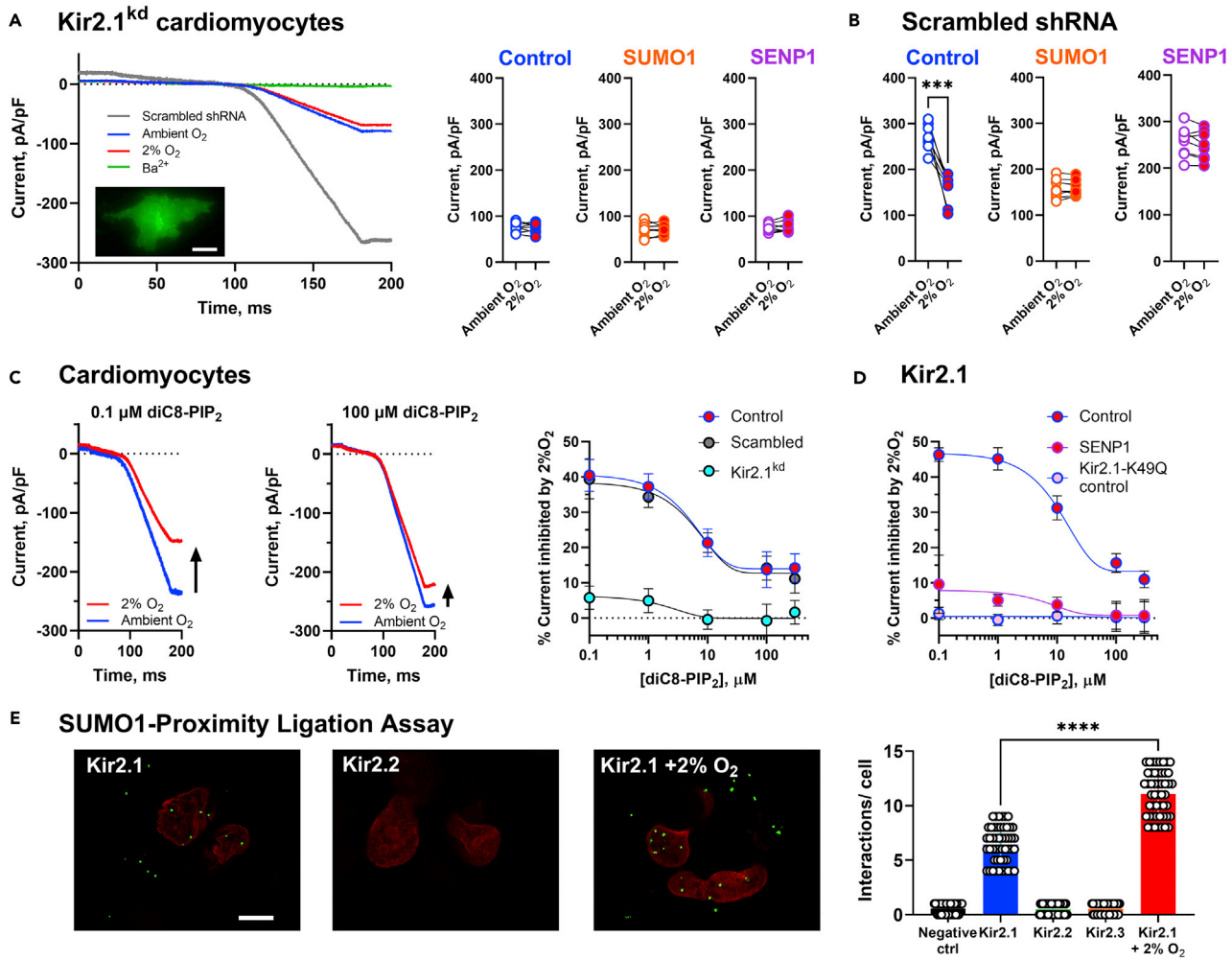

Figure 6. PIP_2 opposed hypoxic inhibition of I_{K1}

I_{K1} was studied in rat ventricular cardiomyocytes (RVCMs) using a whole-cell patch-clamp recording. To the knockdown Kir2.1 expression, RVCMs were transduced with lentiviral particles carrying eGFP and shRNA targeting KCNJ2. Kir2.1 knockdown cells (Kir2.1^{kd}-CMs) were identified by the expression of eGFP. Cells were studied with a control pipette solution (blue), or with pipette solutions containing purified SUMO1 (1 μM, orange) or SENP1 (2 μM, magenta). Where indicated, the control pipette solution contained diC8 PIP_2. Paired patch-clamp data were analyzed by Students *t*-test; ***, $p < 0.01$. The proximity ligation assay (PLA) for native Kir2.1-SUMO1 interactions was performed as described in the STAR Methods and analyzed using an unpaired Mann-Whitney rank test, ****$p < 0.001$. See also Figures S7 and S8.

(A) *Left*, Example sweeps show that I_{K1} is diminished in Kir2.1^{kd}-CMs and the remaining current is insensitive to acute hypoxia. Kir2.1^{kd}-CMs are identified by expression of GFP (*inset*, scale bar = 10 μm). *Right*, summary data from 8 to 10 cells per group show that the regulation of I_{K1} by hypoxia, SUMO1, and SENP1 is lost in Kir2.1^{kd}-CMs.

(B) The magnitude and the regulation of I_{K1} by hypoxia, SUMO1, and SENP1 are unaltered when cells are treated with a control, scrambled shRNA; 7-8 cells per group.

(C) *Left*, Example traces to show that including diC8-PIP_2 in the pipette solution reduces the hypoxic inhibition of I_{K1} in RVCMs in a concentration-dependent manner. The arrow indicates the change in current magnitude between exposure to ambient O_2 and 2% O_2 in the same cell. *Right*, Concentration-response curve showing that including diC8-PIP_2 in the pipette opposes hypoxic inhibition of I_{K1} in control RVCMs and RVCMs expressing the scrambled shRNA. The hypoxic-response is diminished in Kir2.1^{kd}-CMs. Data are mean ± s.d. for 7-8 cells per condition.

(D) DiC8-PIP_2 decreases hypoxic inhibition of Kir2.1 channels expressed in HEK293T cells (control) in a concentration-dependent manner using the experimental paradigm described in C, above. Current inhibition is diminished when SENP1 is included in the recording pipette and is not observed when Kir2.1-K49Q channels are studied. Data are mean ± s.d. for 6 cells per condition.

(E) PLA shows that native Kir2.1 colocalizes with SUMO1 in RVCMs and that Kir2.1-SUMO interactions are increased by acute hypoxia. Kir2.2 and Kir2.3 do not associate with SUMO1. Representative data are shown with DAPI-labeled nuclei in red and PLA interactions in green for ease of visualization. Summary data are obtained from multiple experiments each with multiple fields of view containing 20-30 nuclei. The scale bar is 10 μm.

that does not express I_{K1} under standard culture conditions (Goversen et al., 2018). A direct role of SUMOylation in the hypoxia-induced inhibition of I_{K1} is supported by multiple lines of evidence. Thus, I_{K1} is insensitive to hypoxia in RVCMs studied with SENP1 in the pipette and hypoxic inhibition of the current is reversed by the action of light-activated CRY2-SENP1. I_{K1} is also insensitive to hypoxia in Kir2.1^{kd}-CMs. These findings are recapitulated in our PLA study which further supports that SUMOylation is specific to Kir2.1 and is not observed at Kir2.2 or Kir2.3 channels. SUMOylation of Kir2.1, but not Kir2.2 or 2.3 channel subunits is consistent with our analysis of the SUMO-consensus motif which shows that although all three channels share the first three residues of this sequence, only Kir2.1 has an acidic residue in the fourth position. Intriguingly, when we substituted the asparagine residue in the fourth position of Kir2.2 and Kir2.3 with an aspartic acid we observed SUMO-regulation of channel activity (Figure S5). This finding indicates that it is the lack of the full-canonical consensus SUMO binding site in Kir2.2 and Kir2.3 channels rather than the machinery required to transduce the effects of SUMOylation within the channel that mediates the interplay between the post-translational modification and PIP_2. Lysine 49 is located on the N-terminus of Kir2.1, in close proximity to the PIP_2 binding pocket identified by experimentation and captured in the atomic resolution structure of Kir2.2 (Hansen et al., 2011; Rohacs et al., 2003). Although Lysine 49 is not predicted to interact directly with PIP_2, we speculate that SUMOylation at this residue interferes with interactions between Kir2.1 and PIP_2 that are required for channel function. Given the close proximity between Lysine 49 and residues that interact with PIP_2 (including Lysine 50), the mechanism is likely to be via allosteric modulation of the electrostatic character of the phospholipid binding site.

In addition to the myocardium, Kir2.1 channels are also expressed in skeletal muscle, smooth muscle, bone, immune cells, and diffusely in the cerebral cortex (Hibino et al., 2010), raising the tantalizing possibility that hypoxia-induced SUMOylation plays a more global role in pathophysiology. In contrast, we expect that this mode of regulation would not be observed in cells that predominantly express Kir2.2 or Kir2.3 channels, such as aortic endothelial cells, and neurons in the forebrain, olfactory bulb, and cerebellum (Cui et al., 2021). Of note, Kir2.1 channels are often expressed with other Kir2 family subunits leading to the formation of, at least some, heteromeric channels (Preisig-Muller et al., 2002). Although the SUMO-sensitivity of these complexes is unclear, we speculate that a degree of channel inhibition would occur with a single SUMO-sensitive subunit incorporated into a Kir2 heterotetramer. Thus, we have previously observed that a single SUMOylated K2P1 subunit is sufficient to block the activity of K2P heterodimers in heterologous cells and cerebellar granule neurons and that a single SUMO-sensitive Kv-subunit is sufficient to convey changes in the biophysical properties of Kv2.1, Kv7.1 and I_{Ks} channels (Plant et al., 2010, 2011, 2012; Xiong et al., 2017). Although the SUMO-stoichiometry required to impact the activity of Kir2 channels remains the subject of ongoing investigation, our studies with Kir2.1^{kd}-CMs suggests that at least ~27% of I_{K1} is formed by channels that do not contain SUMO-sensitive Kir2.1 subunits.

We have previously shown that acute hypoxia elicits rapid deployment of SUMO1 to $Na_V1.2$ channels in cerebellar granule neurons and $Na_V1.5$ channels in iPS-derived cardiomyocytes (Plant et al., 2016, 2020). Although the mechanisms that underlie this behavior remain unresolved, it is apparent that the machinery that supports the redistribution of SUMO is conserved and responsive to acute hypoxic challenges across multiple types of cells, including the RVCMs and HEK293T cells, studied here. Given the rapid nature of the hypoxia-response, it is possible that the mobilized pool of SUMO1 is preconjugated to Ubc9; however, we have also previously found evidence for the localization of Ubc9 at the membrane of *Xenopus laevis* oocytes, CHO-K1 cells, and hippocampal neurons (Plant et al., 2010, 2011; Rajan et al., 2005). In common with our study of acute hypoxic challenge, multiple reports have recognized that SUMOs redistribute in cells on exposure to other stressors, including osmotic shock, heat shock, nutrient starvation, and forced gene overexpression, resulting in changes in gene regulation, protein function, and stability (Chymkowitch et al., 2015; Lee et al., 2019; Sramko et al., 2006). Together these findings suggest that the mechanisms that mediate acute hypoxic SUMOylation of Kir2.1 are conserved.

Although SUMOylation regulates the activity of several classes of membrane protein, including K_V, K_{2P}, Na_V, TRP, and ligand-gated channels, the mechanism by which SUMO alters the function of its target proteins has not been elucidated (Benson et al., 2007; Kruse et al., 2009; Martin et al., 2007; Plant et al., 2011, 2012, 2016, 2020). Here, we present multiple lines of evidence to support the conclusion that SUMOylation inhibits Kir2.1 by interfering with channel activation by PIP_2. First, the EC_{50} value for diC8-PIP_2 activation of Kir2.1 is right shifted by SUMOylation (Figure 5). Second, the effectiveness of CRY2-5′ptase to diminish Kir2.1 activity is increased when Kir2.1 is SUMOylated and decreased by SENP1,

consistent with an increase in the lability of PIP_2 (Figure 4). Third, the influence of co-expressed SUMO1 on 5′ptase function is not observed in Kir2.1-K49Q, -K49R, or -D51N channels (Figures 4 and S3), nor does it impact the EC_{50} of diC8-PIP_2 on Kir2.1-K50R channels (Figure 5). Similarly, a single point mutation renders Kir2.2 and 2.3 SUMO-sensitive, suggesting that mechanisms that mediate the functional interaction between SUMO1 and PIP_2 are conserved in the Kir2 channel family (Figure 2). Finally, the hypoxic inhibition of I_{K1} and heterologous Kir2.1 channels is reduced, in a concentration-dependent manner, by exogenous diC8-PIP_2 (Figure 6).

Although we report a SUMO-dependent decrease in the efficacy and potency of diC8-PIP_2 to activate Kir2.1, our data do not determine if SUMOylation changes the affinity between PIP_2 and the channel. Indeed, the potency of diC8-PIP_2 we report here (3.3 μM) is ~7-times greater than the affinity of purified Kir2.1 and a soluble, fluorescent variable of PIP_2 (450 nM) (Cabanos et al., 2017). Functional studies of Kir2.1, considered with the perspective of structural determinations of PIP_2 binding to the closely related Kir2.2 channel (Hansen et al., 2011), have revealed that not all residues required to coordinate PIP_2 impact its efficacy to activate the channel (Donaldson et al., 2003; Lopes et al., 2002; Rohacs et al., 1999, 2003; Soom et al., 2001; Xie et al., 2008; Zhang et al., 1999). The structure of the Kir2.2-PIP_2 complex shows the channel in its closed state; therefore, the apparent dichotomy between structural and functional studies might reflect changes in channel-PIP_2 affinity that occur as the channel visits distinct conformations during gating. Thus, further structure-guided electrophysiological and biochemical studies are required to qualify if SUMOylation acts directly to cause less avid binding of PIP_2, displacement of PIP_2 in the binding pocket, disruption of the electrostatic action of PIP_2 on channel gating, or a change in the activity of other regulatory mechanisms that are not identified in this study. Similarly, whether other SUMO-modified ion channels work by altering interactions with PIP_2 remains to be tested.

Limitations of the study

The data reported in this study are obtained from cultured RVCMs, and heterologous expression of relevant proteins in HEK293T cells or *Xenopus laevis* oocytes. Some limits of this work include that the cardiomyocytes are studied *in vitro* and not within the context of the myocardium, where they would also be exposed to exogenous physiological signals and homeostatic processes. In addition, we study all the cells at room temperature which is expected to slow the kinetics of the interactions under investigation compared to their *in vivo* rates, including SUMOylation and deSUMOylation. Although Kir2.1 is highly dependent on PIP_2 for its activity our optogenetic assessment of SUMO-dependent changes in channel-PIP_2 interactions is, like prior work in the field, correlative based on function and is not a measure of direct binding affinity. However, these data, in concert with our macropatch study, show that SUMOylation reduced the potency and efficacy of PIP_2 to activate Kir2.1 channels. Finally, although I_{K1} was studied using quasi-physiological buffers, the channel was isolated by voltage protocols and drugs that preclude the activation of Ca_V and Na_V channels. We have previously shown that the cardiac sodium channel, $Na_V1.5$, is SUMOylated in response to acute hypoxia (Plant et al., 2020). However, this study does not explore the combined effect of hypoxia-mediated SUMOylation on I_{Na} and I_{K1}.

STAR★METHODS

Detailed methods are provided in the online version of this paper and include the following:

- KEY RESOURCES TABLE
- RESOURCE AVAILABILITY
  - Lead contact
  - Materials availability
  - Data and code availability
- EXPERIMENTAL MODEL AND SUBJECT DETAILS
  - Cell culture
- METHOD DETAILS
  - Reagents
  - Molecular biology and biochemistry
  - Donor-decay FRET
  - Proximity ligation duolink assay
  - Two-electrode voltage-clamp
  - Oocyte macropatch recording

- Whole-cell patch clamp recording
- Generation and delivery of hypoxic perfusate

- QUANTIFICATION AND STATISTICAL ANALYSIS

SUPPLEMENTAL INFORMATION

Supplemental information can be found online at https://doi.org/10.1016/j.isci.2022.104969.

ACKNOWLEDGMENTS

The authors thank members of the Plant and Logothetis labs at Northeastern University for comments on the article. We are grateful to Heikki Vaananen for oocyte preparation and to Dr. Pietro De Camilli for providing CIBN-CAAX and CRY2-5′ptase$_{OCRL}$. The authors thank the CILS core at Northeastern University for confocal microscopy support. The work was funded by National Institutes of Health grant R01HL144615 to L.D.P.

AUTHOR CONTRIBUTIONS

Y.X. and M.M. performed donor-decay FRET. Y.Y. performed Proximity Ligation Assays and confocal microscopy. T.K. performed Western blots. Y.X., A.C., M.M., A.M.B., and T.K. performed molecular biology. Y.X., A.C., K.D.G., M.M., A.M.B., J.G.C., and L.D.P. performed electrophysiology studies. All authors designed experiments and analyzed the data. Y.X., K.D.G, and L.D.P. prepared Figures and wrote the article. All authors reviewed and approved the final version of the article.

DECLARATION OF INTERESTS

The authors report no competing financial interests.

Received: October 13, 2021
Revised: May 7, 2022
Accepted: August 12, 2022
Published: September 16, 2022

REFERENCES

An, H.L., Lu, S.Q., Li, J.W., Meng, X.Y., Zhan, Y., Cui, M., Long, M., Zhang, H.L., and Logothetis, D.E. (2012). The cytosolic GH loop regulates the phosphatidylinositol 4, 5-bisphosphate-induced gating kinetics of Kir2 channels. J. Biol. Chem. *287*, 42278–42287. https://doi.org/10.1074/jbc.M112.418640.

Austen, W.G., Ebert, P.A., and Greenfield, L.J. (1963). Mechanism of cardiac arrest in acute hypoxia. Surgery *53*, 784–791.

Benson, M.D., Li, Q.J., Kieckhafer, K., Dudek, D., Whorton, M.R., Sunahara, R.K., Iñiguez-Lluhí, J.A., and Martens, J.R. (2007). SUMO modification regulates inactivation of the voltage-gated potassium channel Kv1.5. Proc. Natl. Acad. Sci. USA *104*, 1805–1810. https://doi.org/10.1073/pnas.0606702104.

Cabanos, C., Wang, M., Han, X., and Hansen, S.B. (2017). A soluble fluorescent binding assay reveals PIP2 antagonism of TREK-1 channels. Cell Rep. *20*, 1287–1294. https://doi.org/10.1016/j.celrep.2017.07.034.

Chymkowitch, P., Nguéa, A.P., Aanes, H., Koehler, C.J., Thiede, B., Lorenz, S., Meza-Zepeda, L.A., Klungland, A., and Enserink, J.M. (2015). Sumoylation of Rap1 mediates the recruitment of TFIID to promote transcription of ribosomal protein genes. Genome Res. *25*, 897–906. https://doi.org/10.1101/gr.185793.114.

Cui, M., Cantwell, L., Zorn, A., and Logothetis, D.E. (2021). Kir channel molecular physiology, pharmacology, and therapeutic implications. Handb. Exp. Pharmacol. *267*, 277–356. https://doi.org/10.1007/164_2021_501.

Dhamoon, A.S., and Jalife, J. (2005). The inward rectifier current (Ik1) controls cardiac excitability and is involved in arrhythmogenesis. Heart Rhythm *2*, 316–324. https://doi.org/10.1016/j.hrthm.2004.11.012.

Donaldson, M.R., Jensen, J.L., Tristani-Firouzi, M., Tawil, R., Bendahhou, S., Suarez, W.A., Cobo, A.M., Poza, J.J., Behr, E., Wagstaff, J., et al. (2003). PIP2 binding residues of Kir2.1 are common targets of mutations causing Andersen syndrome. Neurology *60*, 1811–1816. https://doi.org/10.1212/01.wnl.0000072261.14060.47.

Edelstein, A.D., Tsuchida, M.A., Amodaj, N., Pinkard, H., Vale, R.D., and Stuurman, N. (2014). Advanced methods of microscope control using muManager software. J. Biol. Methods *1*, e10. https://doi.org/10.14440/jbm.2014.36.

Gada, K.D., Kawano, T., Plant, L.D., and Logothetis, D.E. (2022). An optogenetic tool to recruit individual PKC isozymes to the cell surface and promote specific phosphorylation of membrane proteins. J. Biol. Chem. *298*, 101893. https://doi.org/10.1016/j.jbc.2022.101893.

Goversen, B., van der Heyden, M.A.G., van Veen, T.A.B., and de Boer, T.P. (2018). The immature electrophysiological phenotype of iPSC-CMs still hampers in vitro drug screening: special focus on Ik1. Pharmacol. Ther. *183*, 127–136. https://doi.org/10.1016/j.pharmthera.2017.10.001.

Hansen, S.B., Tao, X., and MacKinnon, R. (2011). Structural basis of PIP2 activation of the classical inward rectifier K+ channel Kir2.2. Nature *477*, 495–498. https://doi.org/10.1038/nature10370.

Hay, R.T. (2005). SUMO: a history of modification. Mol. Cell *18*, 1–12. https://doi.org/10.1016/j.molcel.2005.03.012.

Henley, J.M., Carmichael, R.E., and Wilkinson, K.A. (2018). Extranuclear SUMOylation in neurons. Trends Neurosci. *41*, 198–210. https://doi.org/10.1016/j.tins.2018.02.004.

Hibino, H., Inanobe, A., Furutani, K., Murakami, S., Findlay, I., and Kurachi, Y. (2010). Inwardly rectifying potassium channels: their structure, function, and physiological roles. Physiol. Rev. *90*, 291–366. https://doi.org/10.1152/physrev.00021.2009.

Idevall-Hagren, O., Dickson, E.J., Hille, B., Toomre, D.K., and De Camilli, P. (2012). Optogenetic control of phosphoinositide metabolism. Proc. Natl. Acad. Sci. USA *109*, E2316–E2323. https://doi.org/10.1073/pnas.1211305109.

Kruse, M., Schulze-Bahr, E., Corfield, V., Beckmann, A., Stallmeyer, B., Kurtbay, G., Ohmert, I., Schulze-Bahr, E., Brink, P., and Pongs, O. (2009). Impaired endocytosis of the ion channel TRPM4 is associated with human progressive familial heart block type I. J. Clin. Invest. *119*, 2737–2744. https://doi.org/10.1172/JCI38292.

Lee, A., Zhu, Y., Sabo, Y., and Goff, S.P. (2019). Embryonic cells redistribute SUMO1 upon forced SUMO1 overexpression. mBio *10*, e01856-19. https://doi.org/10.1128/mBio.01856-19.

Liang, S., Wang, Q., Zhang, W., Zhang, H., Tan, S., Ahmed, A., and Gu, Y. (2014). Carbon monoxide inhibits inward rectifier potassium channels in cardiomyocytes. Nat. Commun. *5*, 4676. https://doi.org/10.1038/ncomms5676.

Logothetis, D.E., Petrou, V.I., Zhang, M., Mahajan, R., Meng, X.Y., Adney, S.K., Cui, M., and Baki, L. (2015). Phosphoinositide control of membrane protein function: a Frontier led by studies on ion channels. Annu. Rev. Physiol. *77*, 81–104. https://doi.org/10.1146/annurev-physiol-021113-170358.

Lopes, C.M.B., Zhang, H., Rohacs, T., Jin, T., Yang, J., and Logothetis, D.E. (2002). Alterations in conserved Kir channel-PIP2 interactions underlie channelopathies. Neuron *34*, 933–944.

Martin, S., Nishimune, A., Mellor, J.R., and Henley, J.M. (2007). SUMOylation regulates kainate-receptor-mediated synaptic transmission. Nature *447*, 321–325. https://doi.org/10.1038/nature05736.

Ningoo, M., Plant, L.D., Greka, A., and Logothetis, D.E. (2021). PIP2 regulation of TRPC5 channel activation and desensitization. J. Biol. Chem. *296*, 100726. https://doi.org/10.1016/j.jbc.2021.100726.

Pettersen, E.F., Goddard, T.D., Huang, C.C., Couch, G.S., Greenblatt, D.M., Meng, E.C., and Ferrin, T.E. (2004). UCSF Chimera–a visualization system for exploratory research and analysis. J. Comput. Chem. *25*, 1605–1612. https://doi.org/10.1002/jcc.20084.

Plant, L.D., Dementieva, I.S., Kollewe, A., Olikara, S., Marks, J.D., and Goldstein, S.A.N. (2010). One SUMO is sufficient to silence the dimeric potassium channel K2P1. Proc. Natl. Acad. Sci. USA *107*, 10743–10748. https://doi.org/10.1073/pnas.1004712107.

Plant, L.D., Dowdell, E.J., Dementieva, I.S., Marks, J.D., and Goldstein, S.A.N. (2011). SUMO modification of cell surface Kv2.1 potassium channels regulates the activity of rat hippocampal neurons. J. Gen. Physiol. *137*, 441–454. https://doi.org/10.1085/jgp.201110604.

Plant, L.D., Marks, J.D., and Goldstein, S.A. (2016). SUMOylation of $Na_V1.2$ channels mediates the early response to acute hypoxia in central neurons. Elife *5*, e20054. https://doi.org/10.7554/eLife.20054.

Plant, L.D., Xiong, D., Romero, J., Dai, H., and Goldstein, S.A.N. (2020). Hypoxia produces pro-arrhythmic late sodium current in cardiac myocytes by SUMOylation of NaV1.5 channels. Cell Rep. *30*, 2225–2236.e4. https://doi.org/10.1016/j.celrep.2020.01.025.

Plant, L.D., Zuniga, L., Araki, D., Marks, J.D., and Goldstein, S.A.N. (2012). SUMOylation silences heterodimeric TASK potassium channels containing K2P1 subunits in cerebellar granule neurons. Sci. Signal. *5*, ra84. https://doi.org/10.1126/scisignal.2003431.

Preisig-Müller, R., Schlichthörl, G., Goerge, T., Heinen, S., Brüggemann, A., Rajan, S., Derst, C., Veh, R.W., and Daut, J. (2002). Heteromerization of Kir2.x potassium channels contributes to the phenotype of Andersen's syndrome. Proc. Natl. Acad. Sci. USA *99*, 7774–7779. https://doi.org/10.1073/pnas.102609499.

Rajan, S., Plant, L.D., Rabin, M.L., Butler, M.H., and Goldstein, S.A.N. (2005). Sumoylation silences the plasma membrane leak K^+ channel K2P1. Cell *121*, 37–47. https://doi.org/10.1016/j.cell.2005.01.019.

Rohács, T., Chen, J., Prestwich, G.D., and Logothetis, D.E. (1999). Distinct specificities of inwardly rectifying K(+) channels for phosphoinositides. J. Biol. Chem. *274*, 36065–36072.

Rohács, T., Lopes, C.M.B., Jin, T., Ramdya, P.P., Molnár, Z., and Logothetis, D.E. (2003). Specificity of activation by phosphoinositides determines lipid regulation of Kir channels. Proc. Natl. Acad. Sci. USA *100*, 745–750. https://doi.org/10.1073/pnas.0236364100.

Roy, S., Khanna, S., Bickerstaff, A.A., Subramanian, S.V., Atalay, M., Bierl, M., Pendyala, S., Levy, D., Sharma, N., Venojarvi, M., et al. (2003). Oxygen sensing by primary cardiac fibroblasts: a key role of p21(Waf1/Cip1/Sdi1). Circ. Res. *92*, 264–271. https://doi.org/10.1161/01.res.0000056770.30922.e6.

Sattler, S.M., Skibsbye, L., Linz, D., Lubberding, A.F., Tfelt-Hansen, J., and Jespersen, T. (2019). Ventricular arrhythmias in first acute myocardial infarction: epidemiology, mechanisms, and interventions in large animal models. Front. Cardiovasc. Med. *6*, 158. https://doi.org/10.3389/fcvm.2019.00158.

Schneider, C.A., Rasband, W.S., and Eliceiri, K.W. (2012). NIH Image to ImageJ: 25 years of image analysis. Nat. Methods *9*, 671–675. https://doi.org/10.1038/nmeth.2089.

Soom, M., Schönherr, R., Kubo, Y., Kirsch, C., Klinger, R., and Heinemann, S.H. (2001). Multiple PIP2 binding sites in Kir2.1 inwardly rectifying potassium channels. FEBS Lett. *490*, 49–53. https://doi.org/10.1016/s0014-5793(01)02136-6.

Sramko, M., Markus, J., Kabát, J., Wolff, L., and Bies, J. (2006). Stress-induced inactivation of the c-Myb transcription factor through conjugation of SUMO-2/3 proteins. J. Biol. Chem. *281*, 40065–40075. https://doi.org/10.1074/jbc.M609404200.

Tawil, R., Ptacek, L.J., Pavlakis, S.G., DeVivo, D.C., Penn, A.S., Ozdemir, C., and Griggs, R.C. (1994). Andersen's syndrome: potassium-sensitive periodic paralysis, ventricular ectopy, and dysmorphic features. Ann. Neurol. *35*, 326–330. https://doi.org/10.1002/ana.410350313.

Xie, L.H., John, S.A., Ribalet, B., and Weiss, J.N. (2008). Phosphatidylinositol-4, 5-bisphosphate (PIP2) regulation of strong inward rectifier Kir2.1 channels: multilevel positive cooperativity. J. Physiol. *586*, 1833–1848. https://doi.org/10.1113/jphysiol.2007.147868.

Xiong, D., Li, T., Dai, H., Arena, A.F., Plant, L.D., and Goldstein, S.A.N. (2017). SUMOylation determines the voltage required to activate cardiac IKs channels. Proc. Natl. Acad. Sci. USA *114*, E6686–E6694. https://doi.org/10.1073/pnas.1706267114.

Xu, Y., Cantwell, L., Molosh, A.I., Plant, L.D., Gazgalis, D., Fitz, S.D., Dustrude, E.T., Yang, Y., Kawano, T., Garai, S., et al. (2020). The small molecule GAT1508 activates brain-specific GIRK1/2 channel heteromers and facilitates conditioned fear extinction in rodents. J. Biol. Chem. *295*, 3614–3634. https://doi.org/10.1074/jbc.RA119.011527.

Xu, Z., Lam, L.S.M., Lam, L.H., Chau, S.F., Ng, T.B., and Au, S.W.N. (2008). Molecular basis of the redox regulation of SUMO proteases: a protective mechanism of intermolecular disulfide linkage against irreversible sulfhydryl oxidation. FASEB J *22*, 127–137. https://doi.org/10.1096/fj.06-7871com.

Zaritsky, J.J., Redell, J.B., Tempel, B.L., and Schwarz, T.L. (2001). The consequences of disrupting cardiac inwardly rectifying K(+) current (I(K1)) as revealed by the targeted deletion of the murine Kir2.1 and Kir2.2 genes. J. Physiol. *533*, 697–710. https://doi.org/10.1111/j.1469-7793.2001.t01-1-00697.x.

Zhang, H., He, C., Yan, X., Mirshahi, T., and Logothetis, D.E. (1999). Activation of inwardly rectifying K+ channels by distinct PtdIns(4, 5)P2 interactions. Nat. Cell Biol. *1*, 183–188. https://doi.org/10.1038/11103.

STAR★METHODS

KEY RESOURCES TABLE

REAGENT or RESOURCE	SOURCE	IDENTIFIER
Antibodies		
Kir2.1 potassium channel antibody	Neuromab	Cat# 75–210, RRID:AB_11000720
Kir2.2 potassium channel antibody	Neuromab	Cat# 75–203, RRID:AB_2130486
Kir2.3 potassium channel antibody	Neuromab	Cat# 75-069, RRID:AB_2130742
Rabbit recombinant Anti-Sumo 1 antibody	Abcam	Cat# ab32058, RRID:AB_778173
Bacterial and virus strains		
Kcnj2-Rat shRNA lentiviral particles	OriGene	Cat# TL710087V
Lentiviral shRNA scramble control particles	OriGene	Cat# TR30021V
Chemicals, peptides, and recombinant proteins		
Human SUMO1	Boston Biochemical	Cat# UL-712
Human His_6-SENP1	Boston Biochemical	Cat# E700
Rat Cardiomyocyte Growth Medium (rCGM) BulletKit	Lonza Biosciences	Cat# CC-4515
diC8-PIP_2	Echelon Biosciences	CAS#: 204858-53-7
Wortmannin	Alfa Aesar	CAS#: 19545-26-7
Critical commercial assays		
Duolink(TM) *In Situ* Red Starter Kit Mouse/Rabbit	Sigma-Aldrich	DUO92101-1KT
mMESSAGE mMACHINE™ T7 Transcription Kit	Thermo Fisher Scientific	Cat# AM1344
Experimental models: Cell lines		
Rat ventricular cardiomyocytes from neonatal Wistar rats	Lonza Biosciences	Cat# R-CM-561
Human embryonic kidney (HEK293T) cells	ATCC	CRL-3216
Kir2.1KD Rat ventricular cardiomyocytes	This paper	N/A
Oligonucleotides		
mTFP1-C-F: CCACGACAAGGACTACAACA	This paper	N/A
rIRK1_V48L-F: CAGGAGCCGCTTTCTGAAGAAAGACGGG	This paper	N/A
rIRK1_V48L-R: CCGTCTTTCTTCAGAAAGCGGCTCCTG	This paper	N/A
rIRK1_V48Q-F: GCAGGAGCCGCTTTCAGAAGAAAGACGGGC	This paper	N/A
rIRK1_V48Q-R: GCCCGTCTTTCTTCTGAAAGCGGCTCCTGC	This paper	N/A
rIRK1_V49Q-F: CAGGAGCCGCTTTGTGCAGAAAGACGGGCATTG	This paper	N/A
rIRK1_V49Q-R: CAATGCCCGTCTTTCTGCACAAAGCGGCTCCTG	This paper	N/A
rIRK1_V49R-F: GAGCCGCTTTGTGAGGAAAGACGGGCATTG	This paper	N/A

(*Continued on next page*)

Continued

REAGENT or RESOURCE	SOURCE	IDENTIFIER
rIRK1_V49R-R: CAATGCCCGTCTTTCCTCACAAAGCGGCTC	This paper	N/A
rIRK1_K50A-F: GAGCCGCTTTGTGAAGGCAGACGGGCATTGCAAC	This paper	N/A
rIRK1_K50A-R: GTTGCAATGCCCGTCTGCCTTCACAAAGCGGCTC	This paper	N/A
rIRK1_K50R-F: CCGCTTTGTGAAGAGAGACGGGCATTGC	This paper	N/A
rIRK1_K50R-R: GCAATGCCCGTCTCTCTTCACAAAGCGG	This paper	N/A
rIRK1_K50Q-F: CCGCTTTGTGAAGCAAGACGGGCATTGC	This paper	N/A
rIRK1_K50Q-R: GCAATGCCCGTCTTGCTTCACAAAGCGG	This paper	N/A
rIRK1_D51N-F: GCCGCTTTGTGAAGAAAAACGGGCATTGCAACGTTC	This paper	N/A
rIRK1_D51N-R: GAACGTTGCAATGCCCGTTTTTCTTCACAAAGCGGC	This paper	N/A
rIRK2_N50D-F: GTCAAGAAGGACGGTCAGTGCAACATTGAGTTCGCCAAC	This paper	N/A
rIRK2_N50D-R: GTTGGCGAACTCAATGTTGCACTGACCGTCCTTCTTGAC	This paper	N/A
rIRK3_N25D-F: CGCTTCGTCAAGAAGGACGGCCAGTGCAAC	This paper	N/A
rIRK3_N25D-R: GTTGCACTGGCCGTCCTTCTTGACGAAGCG	This paper	N/A
Recombinant DNA		
Full-length rat Kir2.1 subunit	This paper	GenBank: NM_017296.1
Full-length rat Kir2.2 subunit	This paper	GenBank: NM_053981.2
Full-length rat Kir2.3 subunit	This paper	GenBank: NM_053870.3
mTFP1- full-length rat Kir2.1 subunit	This paper	N/A
mTFP1- full-length rat Kir2.2 subunit	This paper	N/A
mTFP1- full-length rat Kir2.3 subunit	This paper	N/A
SUMO1	This paper	GenBank: NM_003352.8
YFP-SUMO1	This paper	N/A
Ubc9	This paper	GenBank: NM_003345.5
SENP1	This paper	GenBank: NM_001267594.2
CRY2-SENP1	This paper	
CIBN-CAAX	De Camilli lab	Idevall-Hagren et al. (2012)
mCherry-CRY2-5′ptase$_{OCRL}$	De Camilli lab	Idevall-Hagren et al. (2012)
CRY2-5′ptase$_{OCRL}$	This paper	N/A
Software and algorithms		
ImageJ	Schneider et al. (2012)	https://imagej.nih.gov/ij/
Zen Blue	Carl Zeiss Microscopy	https://www.zeiss.com/microscopy/us/products/
WinWCP	Spider	https://spider.science.strath.ac.uk/sipbs/software_winWCP.htm

(*Continued on next page*)

Continued

REAGENT or RESOURCE	SOURCE	IDENTIFIER
WINEDR	Spider	https://spider.science.strath.ac.uk/sipbs/software_winEDR.htm
Clampfit	Molecular Devices,	https://www.moleculardevices.com/products
GraphPad Prism 9.3.1	GraphPad Software, LLC	https://www.graphpad.com/
UCSF Chimera	Pettersen et al. (2004)	https://www.rbvi.ucsf.edu/chimera
μ-manager	Edelstein et al. (2014)	https://micro-manager.org/

RESOURCE AVAILABILITY

Lead contact

Further Information and requests for resources and reagents should be directed to the lead contact, L.D. Plant (l.plant@northeastern.edu).

Materials availability

Materials generated through this work are available from the lead contact upon reasonable request.

Data and code availability

- All data produced in this study are included in the published article and its supplementary information, or are available from the lead contact upon request.
- This paper does not report original code.
- Any additional information required to reanalyze the data reported in this paper is available from the lead contact upon request.

EXPERIMENTAL MODEL AND SUBJECT DETAILS

Cell culture

Rat ventricular cardiomyocytes from neonatal Wistar rats were purchased from Lonza Biosciences. Cells were seeded at 300,000/cm^2 on 1% fibronectin coated coverslips or culture dishes (Thermo Fisher Scientific) and were maintained according to the manufactures instructions in Bullet complete medium (Lonza) supplemented with 200 μM bromo-uridine, to inhibit the proliferation of cardiac fibroblasts. Human embryonic kidney (HEK293T) cells were acquired from American Type Culture Collection (ATCC) and were maintained in Dulbecco's modified Eagle's medium (ATCC) supplemented with 100 units/mL penicillin, 100 μg/mL streptomycin, and 10% (vol/vol) fetal bovine serum. All cells were incubated in a 37°C, humified incubator supplemented with 5% CO_2. Where indicated, cells were cultured at 7% O_2 in a hypoxia-capable tri-gas incubator (Thermo). To study light-activation of CRY2-SENP1, cardiomyocytes were transfected with 1 μg of each of the plasmids indicated using Neuromag magnetic transfection (Oz-biosciences) 24–30 h prior to patch-clamp studies. Transfected cells were identified using mCherry fluorescence. Kir2.1^{KD} cardiomyocytes were generated by applying verified lentiviral particles 36 h prior to the experiment and were identified in culture by eGFP fluorescence. All cardiomyocytes studied by patch-clamp were identified by their beating phenotype. HEK293T cells were transfected using polyethylenimine solution (1 mg/mL) at a ratio of 6 μL per 1 μg of plasmid DNA, 24–30 h prior to experiments. For patch-clamp, FRET and control experiments, we transfect 1 μg of each plasmid DNA, as indicated. Cells for study were identified by expression of a fluorescence marker, as indicated.

METHOD DETAILS

Reagents

Purified SUMO1 and SENP1 were purchased from Boston Biochemical. Purified diC8-PIP_2 was purchased from Echelon Biosciences. Lentiviral particles containing verified shRNA targeted to rat KCNJ2, or a scrambled sequence, were from Origene. Monoclonal antibodies against Kir2.1 (RRID: AB_11000720, Kir2.2 (RRID: AB_2130486), and Kir2.3 (RRID: AB_2130742) were purchased from Neuromab and the polyclonal antibody for SUMO1 [Y299] (ab32058) was obtained from Abcam. The components of the Proximity Ligation Assay (DUO92101) and all other chemical reagents were purchased from Sigma-Aldrich.

Molecular biology and biochemistry

SUMO1 (GenBank: NM_003352.8), Ubc9 (GenBank: NM_003345.5), SENP1 (GenBank: NM_001267594.2) were handled in pMAX, a CMV-based in-house vector (Plant et al., 2020). Rat Kir2.1, Kir2.2 and Kir2.3 (NM_017296.1, NM_053981.2, NM_053870.3) were handled in pCMV5 and pMAX for patch-clamp of HEK293T cells or to generate cRNA for subsequent two-electrode voltage-clamp recording from *Xenopus* oocytes, respectively. The mTFP1-Kir2 constructs were in pMAX. Sequences encoding eYFP or mTFP1 were inserted at the N terminus of SUMO1 or the Kir2 channels, respectively. Mutations were introduced with Quikchange (Agilent) and verified by sequencing (Psomagen, Inc). CIBN-CAAX and mCherry-CRY2-5′ptase$_{OCRL}$ were kind gifts from the De Camilli lab and are characterized in (Idevall-Hagren et al., 2012). The open reading frames of each construct were subcloned into pMAX to facilitate cRNA transcription for studies in *Xenopus laevis* oocytes. CRY2-SENP1 was generated by replacing 5′ptase with SENP1 by ligation. The specificity of the Kir2 channel antibodies was confirmed by Western blot. Briefly, HEK293T cells were seeded in a 24-well plate and transfected with Kir2.1, Kir2.2 or 2.3. After 48 h, total cell lysates were subjected to SDS_PAGE. Proteins of interest were transferred onto a PVDF membrane and detected using monoclonal antibodies raised against rat Kir2.X channels, as indicated.

Donor-decay FRET

Donor-decay time-course Förster Resonance Energy Transfer (FRET) was performed using an Olympus inverted epi-fluorescence microscope. HEK293T cells were transfected with the subunits indicated 24–30 h prior to an experiment and studied in a solution comprising, in mM: NaCl 130, KCl 4, $MgCl_2$ 1.2, $CaCl_2$ 2, HEPES 10, pH was adjusted to 7.4 with NaOH. Regions of interest for study were first identified by YFP fluorescence using a 495/20 nm excitation filter and a 540/30 nm emission filter (Chroma). To assess donor-decay, mTFP1 was subjected to continuous excitation from a broad-spectrum LED (Excelitas) through a 436/20 nm filter using a 20× objective lens (Olympus). The output at the sample was measured at 50 mW/cm^2 by a light meter (ThorLabs). The emission was collected through a 480/40 nm bandpass filter (Chroma). Images were captured every 3 s using a sCMOS camera (Hamamatsu) controlled by μ-manager software (Edelstein et al., 2014). The exposure time was 300 ms. Images were saved as stack files and processed in ImageJ (Schneider et al., 2012). Briefly, the mean fluorescence intensity of discrete areas of membrane, 3–5 nm in length was plotted against time and fit with a mono-exponential decay function to obtain the time constant for decay (τ_{DECAY}). 3–5 regions of interest from 24-35 cells were studied, generating 70–150 τ_{DECAY} values per condition.

Proximity ligation duolink assay

RVCM and HEK-293T cells were fixed by 4% paraformaldehyde (PFA) and permeabilized by 0.2% Triton X-100. Primary antibodies for Kir2.1 (1:200), Kir2.2 (1:200), Kir2.3 (1:200), SUMO1 (Y299, 1:250) were diluted in phosphate buffered saline and applied to the fixed cells at 4°C and incubated overnight. PLA assay kit (Sigma Aldrich, DUO92101) was used according to the manufacturer's instructions. For negative control groups, antibodies against Kir channels were not used. Confocal pictures were captured on a Zeiss LSM880 microscope and analyzed by ZenBlue software (Zeiss) and ImageJ. Briefly, 600 nm confocal slices were used to capture the top of the cells in a field of view, including the plasma membrane and the upper portion of the nucleus. Fluorescence signals indicating ligation between SUMO1 and the Kir2 channel of interest were collected through a Texas Red filter set (Zeiss, set 31) and nuclei were captured using DAPI. Images were subjected to thresholding to remove signals below the background image intensity. The number of cells in each region of interest was determined by counting DAPI stained nuclei. Experiments were repeated at least three times to obtain overall PLA interactions as a function of the number of nuclei. Each field of view contains 20–30 nuclei. The image data shown are from a field of representative cells that is pseudo colored so that the nucleus is red and the PLA interactions are green for clarity. The specificity of the monoclonal Kir2 antibodies for each channel isoform was confirmed by Western blot, as described in the Molecular biology and biochemistry methods.

Two-electrode voltage-clamp

Plasmid DNAs of Kir channel, SUMO1, Ubc9, SENP1, CIBN-CAAX and CRY2-5′ptase$_{OCRL}$ were linearized prior to *in vitro* transcription. Capped RNAs were transcribed using mMessage mMachine T7 transcription kit (Thermo Fisher Scientific). *Xenopus* oocytes were surgically extracted in accord with an IACUC protocol at Northeastern University. Oocytes were then dissociated, and defolliculated by collagenase treatment and microinjected with 50 nL of a RNAse/DNAse free water solution per oocyte containing the required

cRNAs: we injected 1 ng channel, 5 ng SUMO1, 1 ng ubc9, 1 ng SENP1, 1 ng CRY2-5'ptase and 1 ng CIBN-CAAX, as indicated for two-electrode voltage-clamp experiments, oocytes were incubated for 1–2 days at 17°C before currents were recorded. Electrodes were pulled using a Flaming-Brown micropipette puller (Sutter Instruments) and were filled with 3 M KCl in 1.5% (w/v) agarose to give resistances between 0.5 and 1.0 MΩ. The oocytes were bathed in ND96 recording solution comprising, in mM: KCl 2, NaCl 96, $MgCl_2$ 1, and HEPES 5, buffered to pH 7.4 with KOH. Where indicated, Kir2 channel currents were assessed in a high-K^+ recording solution comprising, in mM: KCl 96, NaCl 2, $MgCl_2$ 1, and HEPES 5, buffered to pH 7.4 with KOH. Whole oocyte currents were measured using a GeneClamp 500 (Molecular Devices) amplifier, controlled via a USB interface (National Instruments), and were recorded using WinWCP software (University of Strathclyde). To study Kir2 channels, oocytes were held at 0 mV, and currents were assessed by 160-ms ramps from −80 to +80 mV that were repeated every second. The 5-ptase$_{OCRL}$ system was activated using a 460 nm LED (Luminus) that was focused on the oocytes using a collimating lens (ThorLabs). At the end of the study, currents were blocked by 10 mM $BaCl_2$. The Ba^{2+}-sensitive component of the current was analyzed. The data are expressed as peak current before activation of the 460 nm LED, the percentage of current remaining at the end of the inhibition, and the time constant of the inhibition (tau), determined by a mono-exponential fit function in Clampfit software (Molecular Devices). Between 4 and 12 oocytes from at least two different *Xenopus* frogs were studied per experiment.

Oocyte macropatch recording

Macropatch Kir2.1 channel currents were recorded from devitellinized oocytes by patch-clamp in the inside-out mode using an AM2400 patch-clamp amplifier (A-M Systems). Currents were digitized using a USB-interface (National Instruments) and WinEDR (University of Strathclyde) data acquisition software. Electrodes were fabricated using Kimax glass (WPI) and had a resistance of 0.5–1 MΩ when filled with an recording buffer containing (in mM): 96 KCl, 1 $MgCl_2$, and 5 HEPES at pH 7.4. Oocytes were bathed with a solution comprising (in mM): 96 KCl, 5 EGTA, 1 MgATP, and 10 HEPES at pH 7.4. The current amplitude was measured at 100 mV with a sampling rate of 10 kHz. Data were analyzed using WinEDR and Clampfit software (Molecular Devices). Once a patch was excised, the bath solution was replaced with one containing poly-L-lysine (20 μg/mL; PLL) until a stable baseline was achieved (typically 30–60 s). Then, patches were exposed to increasing concentrations of diC8-PIP_2. Patches were typically stable for long enough to allow 5–7 concentrations of diC8-PIP_2 to reach equilibrium. Therefore, each experiment contained a reference of 10 μM diC8-PIP_2 to allow for comparison between patches. EC_{50} was defined as the concentration of diC8-PIP_2 required to activate half of the Kir2.1 current.

Whole-cell patch clamp recording

Whole-cell currents were recorded with a Tecella Pico-2 amplifier (Tecella) controlled using WinWCP software (Spider, University of Strathclyde). Currents were acquired through a low-pass Bessel filter at 2 kHz and were digitized at 10 kHz. Patch pipettes were fabricated from borosilicate glass (Clark Kent), using a vertical puller (Narishige) and had a resistance of 2.5–4 MΩ when filled with the intracellular buffers described below. To study I_{K1} in cardiomyocytes, the recording pipettes were filled with a solution comprising, in mM: K-aspartate 100, KCl 40, $MgCl_2$ 5, EGTA 5, Na_2ATP 5, and HEPES 5, adjusted to pH 7.2 (KOH). Cardiomyocytes were identified morphologically, by expression of eGFP (where indicated) and by their beating behavior. Cardiac fibroblasts had a distinct morphology, did not beat and were not observed to pass I_{K1} current when they were studied by whole-cell patch-clamp recording (data not shown). The cells were initially bathed in a solution comprising, in mM: NaCl 140, KCl 5, $MgCl_2$ 1, mM $CaCl_2$ 1.8, glucose 10, and HEPES 5, adjusted to pH 7.4 (NaOH). To patch-clamp beating cells, the recording pipette was brought close to the cell of interest and prior to making contact, 10 μM nitrendipine was added to the recording solution to block Ca^{2+} flux through Ca_V channels. Following break through into whole-cell mode, cardiomyocytes were allowed to stabilize for 2 min then I_{K1} currents was assessed by holding at 0 mV then stepping to +40 mV for 50 ms before a ramp to −120 mV at a rate of 1 mV/ms. The magnitude of I_{K1} was then assessed over 50 ms at −120 mV before the cell returned to the holding potential. The physiological recording buffer was replaced with a high-K^+ buffer comprising, in mM: NaCl 81, KCl 64, $MgCl_2$ 1, $CaCl_2$ 1.8, glucose 10, and HEPES 5, adjusted to pH 7.4 (NaOH). Bath perfusion was via a multichannel gravity-driven perfusion manifold (Warner). This recording protocol, combined with the use of nitrendipine and the high K^+ solution isolated I_{K1} in the native cells (Liang et al., 2014). HEK293T cells heterologously expressing Kir2 channels were studied using an intracellular buffer comprising, in mM: KCl 140, $MgCl_2$ 2, EGTA 1, Na_2ATP 5 and HEPES 5, adjusted to pH 7.2 with KOH. Following break through into whole-cell mode, the cells were allowed to stabilize for 2 min then currents were assessed by ramps from

−80 to +80 mV that were repeated at 1 Hz. The external physiological recording buffer comprised, in mM: NaCl 135, KCl 5, $MgCl_2$ 1.2, $CaCl_2$ 1.5, glucose 8, and HEPES 10, adjusted to pH 7.4 with NaOH, and transitioned to a high-K^+ buffer comprising, in mM: NaCl 5, KCl 135, $MgCl_2$ 1.2, $CaCl_2$ 1.5, glucose 8, and HEPES 10, adjusted to pH 7.4 with KOH. For both native I_{K1} and heterologous Kir2 channel studies the Ba^{2+}-sensitive component of the current was analyzed and determined by perfusing 5mM $BaCl_2$ in the high-K^+ buffer at the end of each experiment. Cells for study were selected based on GFP or mCherry expression using an epifluorescence microscope (Olympus). Rat cardiomyocytes and HEK293T cells had a mean whole-cell capacitance of 32 ± 6 pF and 12 ± 2 pF respectively; series resistance was typically <10 MΩ, and the voltage-error of 3 mV was not compensated.

Generation and delivery of hypoxic perfusate

Acute hypoxia was achieved by switching the perfusate with one that had been bubbled with nitrogen for at least 30 min prior to the experiment. Oxygen tension was measured at the cell by a calibrated oxygen probe (Ocean Insight); solution exchange occurred in less than 20 s via gas impermeable Tygon tubing. For patch-clamp studies, cells were initially studied in a quasi-physiological recording buffer, or a high-K^+ buffer equilibrated to ambient O_2 (21%) or 7% O_2, as indicated. The cells were then exposed to a buffer equilibrated to 2% O2 (acute hypoxia) for the time-indicated. For the PLA study, cells were exposed to hypoxia for 5-min before being immediately fixed in 4% paraformaldehyde. All hypoxic solutions were equilibrated, measured, and perfused at room temperature (~20°C).

QUANTIFICATION AND STATISTICAL ANALYSIS

Data were analyzed using Clampfit, GraphPad (Prism) and Excel software. Quantification and analysis approaches were specific in each experiment and are described in the Figure legends. Data were assessed for statistical differences between groups by unpaired Mann-Whitney rank test or two-tailed Students *t*-test, as indicated in the Figure legends, following interrogation of variance with Bonferroni *post hoc* analysis to test differences within pairs of group means for all dataset with an F-value of $p < 0.05$. Data are presented, where indicated as the mean ± standard deviation (s.d.). The number of replicates for each study are described in the legends.